

**Electron-impact single and double ionization of helium**

M. S. Pindzola, F. Robicheaux, J. P. Colgan,\* M. C. Witthoef, and J. A. Ludlow

*Department of Physics, Auburn University, Auburn, Alabama 36849, USA*

(Received 26 April 2004; published 15 September 2004)

Electron-impact ionization cross sections for helium are calculated using time-dependent close-coupling theory. The total wave function for the three electron system is expanded in nine dimensions, where three dimensions are represented on a radial lattice and a coupled channels expansion is used to represent the other six dimensions. Collision cross sections are obtained by  $t \rightarrow \infty$  projection onto fully antisymmetric spatial and spin functions, with care as to orthogonality of different representations. Cross sections are also obtained using time-independent first- and second-order perturbative distorted-wave theory. Total cross sections are calculated at incident energies above the double ionization threshold for electron-impact single ionization leaving  $\text{He}^+$  in the  $1s$ ,  $2s$ , and  $2p$  states and for electron-impact double ionization. Both the single ionization cross section, leaving  $\text{He}^+$  in the  $1s$  ground state, and the double ionization cross section are in excellent agreement with previous absolute experimental measurements.

DOI: 10.1103/PhysRevA.70.032705

PACS number(s): 34.50.Fa

**I. INTRODUCTION**

A number of nonperturbative theoretical methods have recently been developed that successfully treat two continuum electrons moving in the field of a charged core, that is, Coulomb three-body breakup. The converged close-coupling [1], the hyperspherical close-coupling [2], the  $R$ -matrix pseudostates [3], the time-dependent close-coupling [4], and the exterior complex scaling [5] methods have all obtained total cross sections for the electron-impact ionization of hydrogen that are in excellent agreement with the crossed-beams experiment of Shah *et al.* [6]. To date these nonperturbative methods [7–9] have also successfully calculated the wide range of energy and angle differential cross sections found in the electron induced breakup of the hydrogen atom.

In this paper we develop a nonperturbative theoretical method to treat three continuum electrons moving in the field of a charged core, that is, Coulomb four-body breakup. We apply the method to obtain total cross sections for the electron-impact ionization of helium. For single ionization, leaving  $\text{He}^+$  in the  $1s$  ground state, we can compare to previous nonperturbative methods, which freeze one of the  $K$  shell electrons [10–12], and to absolute experimental measurements [13–15]. For single ionization, leaving  $\text{He}^+$  in the  $2l$  excited states, we can compare to hybrid calculations [16,17], in which the scattered electron is treated by perturbative distorted-wave methods and the inner electrons are treated by a nonperturbative  $R$ -matrix method. In the case of single ionization, leaving  $\text{He}^+$  in the  $2p$  excited state, we can also compare to absolute experimental measurements [18,19]. For double ionization, we can compare to hybrid calculations [20], in which the scattered electron is treated in the plane-wave Born approximation and the inner electrons are treated using perturbation theory to connect correlated

initial and final states, and to absolute experimental measurements [15]. To date the hybrid methods [21–23] have also been successfully extended to calculate a wide range of energy and angle differential cross sections in the electron ionization with excitation and double ionization of helium.

In this paper a nonperturbative close-coupling method is used to solve for the electron ionization of helium at low total angular momentum. A nine-dimensional wave function is propagated in time according to the Schrodinger equation, with the three radial dimensions represented on a numerical lattice and the six angular dimensions represented by a coupled channels expansion. Collision cross sections are obtained by  $t \rightarrow \infty$  projection onto fully antisymmetric spatial and spin functions, with care as to orthogonality of different representations. A perturbative distorted-wave method is then used for the electron ionization of helium at all total angular momentum. Total cross sections are obtained by scaling the approximate perturbative results to match the nonperturbative results at low total angular momentum, and then extrapolating the nonperturbative results using the high total angular momentum scaled perturbative results as a guide. Comparisons are then made with other theoretical methods and absolute experimental measurements. The time-dependent close-coupling and time-independent distorted-wave methods are presented in Sec. II, total single and double ionization cross sections for helium are presented in Sec. III, and a brief summary is found in Sec. IV. Unless otherwise stated, we will use atomic units.

**II. THEORY****A. Time-dependent nonperturbative close-coupling method**

For electron ionization of a two-electron target atom, the angular reduction of the time-dependent Schrödinger equation for a three electron wave function yields a set of time-dependent close-coupled partial differential equations for each  $\mathcal{L}$  symmetry:

---

\*Present address: Theoretical Division, LANL, Los Alamos, NM 87545, USA.

$$\begin{aligned}
 i \frac{\partial P_{l_1 l_2 l_3}^{\mathcal{L}}(r_1, r_2, r_3, t)}{\partial t} &= T_{l_1 l_2 l_3}(r_1, r_2, r_3) P_{l_1 l_2 l_3}^{\mathcal{L}}(r_1, r_2, r_3, t) \\
 &+ \sum_{l'_1, l'_2, l'_3} \sum_{l'_i < j}^3 V_{l_1 l_2 l_3, l'_1 l'_2 l'_3}^{\mathcal{L}}(r_i, r_j) P_{l'_1 l'_2 l'_3}^{\mathcal{L}}(r_1, r_2, r_3, t),
 \end{aligned} \tag{1}$$

where

$$T_{l_1 l_2 l_3}(r_1, r_2, r_3) = \sum_i^3 \left( -\frac{1}{2} \frac{\partial^2}{\partial r_i^2} + \frac{l_i(l_i+1)}{2r_i^2} - \frac{Z}{r_i} \right), \tag{2}$$

and the coupling operators are given in terms of standard  $3j$  and  $6j$  symbols by

$$\begin{aligned}
 V_{l_1 l_2 l_3, l'_1 l'_2 l'_3}^{\mathcal{L}}(r_1, r_2) &= (-1)^{l_1+l'_1+L} \delta_{l_3, l'_3} \delta_{L, L'} \times \sqrt{(2l_1+1)(2l'_1+1)(2l_2+1)(2l'_2+1)} \\
 &\times \sum_{\lambda} \frac{(r_1, r_2)_{\lambda}^{\leq}}{(r_1, r_2)_{\lambda}^{\geq+1}} \begin{pmatrix} l_1 & \lambda & l'_1 \\ 0 & 0 & 0 \end{pmatrix} \begin{pmatrix} l_2 & \lambda & l'_2 \\ 0 & 0 & 0 \end{pmatrix} \begin{Bmatrix} l_1 & l_2 & L \\ l'_2 & l'_1 & \lambda \end{Bmatrix},
 \end{aligned} \tag{3}$$

$$\begin{aligned}
 V_{l_1 l_2 l_3, l'_1 l'_2 l'_3}^{\mathcal{L}}(r_1, r_3) &= (-1)^{l_2+L} \delta_{l_2, l'_2} \sqrt{(2l_1+1)(2l'_1+1)(2l_3+1)(2l'_3+1)(2L+1)(2L'+1)} \\
 &\times \sum_{\lambda} (-1)^{\lambda} \frac{(r_1, r_3)_{\lambda}^{\leq}}{(r_1, r_3)_{\lambda}^{\geq+1}} \begin{pmatrix} l_1 & \lambda & l'_1 \\ 0 & 0 & 0 \end{pmatrix} \begin{pmatrix} l_3 & \lambda & l'_3 \\ 0 & 0 & 0 \end{pmatrix} \begin{Bmatrix} L & l_3 & L \\ l'_3 & L' & \lambda \end{Bmatrix} \begin{Bmatrix} l_1 & l_2 & L \\ L' & \lambda & l'_1 \end{Bmatrix},
 \end{aligned} \tag{4}$$

and

$$\begin{aligned}
 V_{l_1 l_2 l_3, l'_1 l'_2 l'_3}^{\mathcal{L}}(r_2, r_3) &= (-1)^{l'_1+l_2+l'_2+L+L'+L} \delta_{l_1, l'_1} \sqrt{(2l_2+1)(2l'_2+1)(2l_3+1)(2l'_3+1)(2L+1)(2L'+1)} \\
 &\times \sum_{\lambda} (-1)^{\lambda} \frac{(r_2, r_3)_{\lambda}^{\leq}}{(r_2, r_3)_{\lambda}^{\geq+1}} \begin{pmatrix} l_2 & \lambda & l'_2 \\ 0 & 0 & 0 \end{pmatrix} \begin{pmatrix} l_3 & \lambda & l'_3 \\ 0 & 0 & 0 \end{pmatrix} \begin{Bmatrix} L & l_3 & L \\ l'_3 & L' & \lambda \end{Bmatrix} \begin{Bmatrix} l_1 & l_2 & L \\ \lambda & L' & l'_2 \end{Bmatrix}.
 \end{aligned} \tag{5}$$

The initial condition for the solution of the time-dependent close-coupling equations of Eq. (1) is given by

$$P_{l_1 l_2 l_3}^{\mathcal{L}}(r_1, r_2, r_3, t=0) = \sum_l \bar{P}_{ll}^S(r_1, r_2) G_{k_0 \mathcal{L}}(r_3) \delta_{l_1, l} \delta_{l_2, l} \delta_{l_3, \mathcal{L}} \delta_{L, 0}, \tag{6}$$

where the radial wave functions,  $\bar{P}_{ll}^S(r_1, r_2)$ , are obtained by relaxation of the Schrodinger equation in imaginary time for a two-electron target atom [24], and the Gaussian radial wave packet,  $G_{k_0 \mathcal{L}}(r_3)$ , has a propagation energy of  $k_0^2/2$ . The three-electron close-coupling equations of Eq. (1) are a generalization of the two-electron close-coupling equations used before for electron ionization of one active electron target atoms [25–27].

The time-dependent close-coupled equations of Eq. (1) are solved using standard numerical methods to obtain a discrete representation of the radial wave functions and all operators on a three-dimensional lattice. Our specific implementation on massively parallel computers is to partition both the  $r_2$  and  $r_3$  coordinates over the many processors, so-called domain decomposition. At each time step of the solution only those parts of the radial wave functions needed to calculate the second derivatives found in Eq. (2) are passed between the processors.

Probabilities for all the many collision processes possible are obtained by  $t \rightarrow \infty$  projection onto fully antisymmetric spatial and spin wave functions. As an example, for electron double ionization of the  $1S$  ground state of helium, the collision probability is given by

$$\begin{aligned}
P_{l_1 l_2 l_3 \mathcal{L} \frac{1}{2} \frac{1}{2} S \frac{1}{2} \frac{1}{2}}(t) = & \sum_{k_1} \sum_{k_2} \sum_{k_3} \left| \sum_{L'} \delta_{L,L'} Q_a R(123,t) - \sum_{L'} (-1)^{l_2+l_3+L+L'} \sqrt{(2L+1)(2L'+1)} \begin{Bmatrix} l_2 & l_1 & L \\ l_3 & \mathcal{L} & L' \end{Bmatrix} Q_b R(132,t) \right. \\
& - \sum_{L'} (-1)^{l_1+l_2-L'} \delta_{L,L'} Q_c R(213,t) + \sum_{L'} (-1)^{l_1+l_2+L} \sqrt{(2L+1)(2L'+1)} \begin{Bmatrix} l_2 & l_1 & L \\ l_3 & \mathcal{L} & L' \end{Bmatrix} Q_c R(312,t) \\
& + \sum_{L'} (-1)^{l_2+l_3+L'} \sqrt{(2L+1)(2L'+1)} \begin{Bmatrix} l_1 & l_2 & L \\ l_3 & \mathcal{L} & L' \end{Bmatrix} Q_b R(231,t) \\
& \left. - \sum_{L'} \sqrt{(2L+1)(2L'+1)} \begin{Bmatrix} l_1 & l_2 & L \\ l_3 & \mathcal{L} & L' \end{Bmatrix} Q_a R(321,t) \right|^2, \tag{7}
\end{aligned}$$

where

$$\begin{aligned}
R(ijk,t) = & \int_0^\infty dr_1 \int_0^\infty dr_2 \int_0^\infty dr_3 P_{k_1 l_1}(r_i) P_{k_2 l_2}(r_j) \\
& \times P_{k_3 l_3}(r_k) P_{l_1 l_2 L'}^{\mathcal{L}}(r_1, r_2, r_3, t), \tag{8}
\end{aligned}$$

$Q_a = \sqrt{\frac{1}{2}} \delta_{S,0} - \sqrt{\frac{1}{6}} \delta_{S,1}$ ,  $Q_b = \sqrt{\frac{2}{3}} \delta_{S,1}$ , and  $Q_c = -\sqrt{\frac{1}{2}} \delta_{S,0} - \sqrt{\frac{1}{6}} \delta_{S,1}$ . A comparable collision probability expression for electron ionization of the  $^2S$  ground state of hydrogen is much simpler, only the sum or difference of the two-electron radial integrals  $R(12,t)$  and  $R(21,t)$  is needed. In fact, since for two electron systems the spatial and spin wave functions separate, collision probabilities can be easily obtained by projection onto simple products of one-electron radial functions, provided the two electron time-propagated radial wave function is symmetrized for singlet scattering or antisymmetrized for triplet scattering [4].

The radial wave functions,  $P_{ki}(r)$ , are obtained by matrix diagonalization of the radial one electron Hamiltonian:

$$h(r) = -\frac{1}{2} \frac{\partial^2}{\partial r^2} + \frac{l(l+1)}{2r^2} + V(r), \tag{9}$$

where  $V(r) = -Z/r$ . Care must be taken in the sums over the electron momenta  $k_1, k_2, k_3$  found in the collision probability of Eq. (7). When the associated angular momenta are equal, for example  $l_1 = l_2$ , the sums must be restricted to avoid double counting of distinct continuum states. More subtle is the unwanted contribution to the collision probability from the continuum correlation part of the two-electron wave functions. For example, the collision probability of Eq. (7) is nonzero for even the initial radial wave function,  $P_{l_1 l_2 l_3}^{\mathcal{L}}(r_1, r_2, r_3, t=0)$ , of Eq. (6). This point has been discussed in detail by McCurdy *et al.* [28] in a study of the electron double ionization of an  $s$ -wave model He atom. Instead of projecting out two-electron bound states from the three electron time-propagated radial wave function and then projecting onto all electron momenta in Eq. (7), we found that a simple restriction of the sums over the electron momenta, so that the conservation of energy,

$$E_{atom} + \frac{k_0^2}{2} = \frac{k_1^2}{2} + \frac{k_2^2}{2} + \frac{k_3^2}{2}, \tag{10}$$

was approximately conserved, greatly reduced contamination from the continuum piece of the two-electron bound-state wave functions. For example, the electron momenta  $k_i$  in the sum found in Eq. (7) are chosen if half their squared sum is greater than  $(1-\epsilon)(E_{atom} + k_0^2/2)$  and less than  $(1+\epsilon)(E_{atom} + k_0^2/2)$ . Tests show that the cross sections are stable for a range of  $\epsilon$  around 0.30. In addition, this method of restricted momenta sums should become more accurate as the lattice size increases. We note that the collision probability for electron single ionization of the  $^1S$  ground state of helium leaving the  $\text{He}^+$  ion in an  $nl$  bound state is almost identical to Eq. (7). Simply eliminate one of the sums over electron momenta, change one of the  $P_{ki}(r)$  radial wave functions to  $P_{ni}(r)$ , calculate the remaining two continuum radial wave functions in a  $V(r)$  potential that screens the Coulomb field, and apply the relevant equation for the conservation of energy.

Finally, the electron-impact single or double ionization cross section is given by

$$\sigma_e = \frac{\pi}{2k_0^2} \sum_{\mathcal{L}} 2(2\mathcal{L}+1) \sum_{l_1, l_2, l_3, L, S} \mathcal{P}_{l_1 l_2 l_3 \mathcal{L} \frac{1}{2} \frac{1}{2} S \frac{1}{2} \frac{1}{2}}(t \rightarrow \infty). \tag{11}$$

Care must also be taken in the sums over the quantum numbers associated with the fully antisymmetric spatial and spin wave functions found in Eq. (11) to avoid double counting.

### B. Time-independent perturbative distorted-wave method

From perturbation theory the electron-impact single ionization cross section for helium, leaving  $\text{He}^+$  in the  $1s$  ground state, is given by

$$\sigma_{ion} = \int_0^E \frac{8}{k_0^3 k_1 k_2} \sum_{\mathcal{L}} 2(2\mathcal{L}+1) \sum_{l_1} \sum_{l_2} \sum_S |V_{fi}|^2 d(k_1^2/2), \tag{12}$$

where

TABLE I. Electron-impact single ionization cross sections (in kb), leaving He<sup>+</sup> in the 1s ground state, as calculated by the 3D time-dependent close-coupling method, at various incident electron energies (1.0 kb=1.0×10<sup>-21</sup> cm<sup>2</sup>).

$\mathcal{L}$	100.0 eV	150.0 eV	200.0 eV
0	1750	1140	805
1	3080	2130	1560
2	5570	3570	2490
3	6220	4480	3260
4	5120	4200	3240
5	3850	3660	3040

$$E = E_{atom} + \frac{k_0^2}{2} = E_{ion}(1s) + \frac{k_1^2}{2} + \frac{k_2^2}{2}. \quad (13)$$

The first-order scattering potential for the transition  $1s^2 k_0 l_0 \ ^2\mathcal{L} \rightarrow 1s k_1 l_1 \ ^{2S+1}l_1 \ k_2 l_2 \ ^2\mathcal{L}$  is given by

$$V_{fi} = \delta_{l_0, \mathcal{L}} (-1)^{l_1 - l_2} \begin{pmatrix} l_1 & l_2 & l_0 \\ 0 & 0 & 0 \end{pmatrix} \times \left( \sqrt{2} \delta_{S,0} \sqrt{\frac{(2l_2+1)}{(2l_1+1)}} R^{l_1}(k_1 l_1, k_2 l_2, 1s, k_0 l_0) - \sqrt{\frac{(2S+1)}{2}} \sqrt{\frac{(2l_1+1)}{(2l_2+1)}} R^{l_2}(k_1 l_1, k_2 l_2, k_0 l_0, 1s) \right), \quad (14)$$

where the  $R^\lambda(n_1 l_1, n_2 l_2, n_3 l_3, n_4 l_4)$  are standard radial Slater integrals. The 1s bound orbital is calculated in the Hartree-Fock approximation [29], while the  $k_0 l_0$ ,  $k_1 l_1$ , and  $k_2 l_2$  continuum orbitals are calculated in a mixture of  $V^N$  and  $V^{N-1}$  scattering potentials [30].

From perturbation theory the electron-impact single ionization cross section for helium, leaving He<sup>+</sup> in the  $2l$  excited state, is given by

$$\sigma_{ion} = \int_0^E \frac{8}{k_0^3 k_1 k_2} \sum_{\mathcal{L}} 2(2\mathcal{L}+1) \sum_{l_1} \sum_{l_2} \sum_{l_n} \sum_S |V_{fi}|^2 d(k_1^2/2), \quad (15)$$

where

TABLE II. Electron-impact single ionization cross sections (in kb), leaving He<sup>+</sup> in the 2s ground state, as calculated by the 3D time-dependent close-coupling method, at various incident electron energies (1.0 kb=1.0×10<sup>-21</sup> cm<sup>2</sup>).

$\mathcal{L}$	100.0 eV	150.0 eV	200.0 eV
0	7.60	14.9	15.9
1	19.3	28.7	30.0
2	37.6	57.1	54.7
3	26.2	52.8	57.0
4	1.80	14.2	26.9
5	0.59	4.62	14.5

TABLE III. Electron-impact single ionization cross sections (in kb), leaving He<sup>+</sup> in the 2p ground state, as calculated by the 3D time-dependent close-coupling method, at various incident electron energies (1.0 kb=10×10<sup>-21</sup> cm<sup>2</sup>).

$\mathcal{L}$	100.0 eV	150.0 eV	200.0 eV
0	7.28	15.5	16.5
1	21.8	32.3	31.8
2	33.8	41.1	37.7
3	32.2	56.1	54.6
4	50.1	81.1	77.8
5	22.4	63.5	75.4

$$E = E_{atom} + \frac{k_0^2}{2} = E_{ion}(2l) + \frac{k_1^2}{2} + \frac{k_2^2}{2}. \quad (16)$$

The second-order scattering potential for the important transition  $1s^2 k_0 l_0 \ ^2\mathcal{L} \rightarrow 1s k_n l_n \ ^{2S+1}l_n \ k_2 l_2 \ ^2\mathcal{L} \rightarrow 2l k_1 l_1 \ ^{2S+1}l_n \ k_2 l_2 \ ^2\mathcal{L}$  is given by

$$V_{fi} = \delta_{l_0, \mathcal{L}} \sum_{k_n} (-1)^{l-l_1} \begin{pmatrix} l & l_1 & l_n \\ 0 & 0 & 0 \end{pmatrix} (-1)^{l_n - l_2} \begin{pmatrix} l_n & l_2 & l_0 \\ 0 & 0 & 0 \end{pmatrix} \times \left( \sqrt{\frac{(2l_1+1)}{(2l+1)}} R^l(2l, k_1 l_1, 1s, k_n l_n) + (-1)^S \sqrt{\frac{(2l+1)}{(2l_1+1)}} R^{l_1}(2l, k_1 l_1, k_n l_n, 1s) \right) \times \left( \sqrt{2} \delta_{S,0} \sqrt{\frac{(2l_2+1)}{(2l_n+1)}} R^{l_n}(k_n l_n, k_2 l_2, 1s, k_0 l_0) - \sqrt{\frac{(2S+1)}{2}} \sqrt{\frac{(2l_n+1)}{(2l_2+1)}} R^{l_2}(k_n l_n, k_2 l_2, k_0 l_0, 1s) \right) \times \left( E_{atom} + \frac{k_0^2}{2} - E_{ion}(1s) - \frac{k_n^2}{2} - \frac{k_2^2}{2} \right)^{-1}. \quad (17)$$

The 1s, 2l, and  $nl_n$  bound orbitals are hydrogenic, while the  $k_0 l_0$ ,  $k_1 l_1$ ,  $k_2 l_2$ , and  $k_n l_n$  continuum orbitals are calculated in a  $V^{N-1}$  scattering potential.

From perturbation theory the electron-impact double ionization cross section for helium is given by

TABLE IV. Electron-impact double ionization cross sections (in kb), as calculated by the 3D time-dependent close-coupling method, at various incident electron energies (1.0 kb=10×10<sup>-21</sup> cm<sup>2</sup>).

$\mathcal{L}$	100.0 eV	150.0 eV	200.0 eV
0	0.14	2.44	4.74
1	1.63	7.51	10.4
2	2.88	14.2	18.0
3	2.38	17.2	24.3
4	3.09	19.4	26.1
5	0.79	10.4	18.2

$$\sigma_{dion} = \int_0^E \int_0^{E-k_1^2/2} \frac{16}{\pi k_0^3 k_1 k_2 k_3} \sum_{\mathcal{L}} 2(2\mathcal{L}+1) \times \sum_{l_1} \sum_{l_2} \sum_{l_3} \sum_{l_n} \sum_s |V_{fi}|^2 d(k_2^2/2) d(k_1^2/2), \quad (18)$$

where

$$E = E_{atom} + \frac{k_0^2}{2} = \frac{k_1^2}{2} + \frac{k_2^2}{2} + \frac{k_3^2}{2}. \quad (19)$$

The second-order scattering potential for the important transition  $1s^2 k_0 l_0 \ ^2\mathcal{L} \rightarrow 1s k_n l_n \ ^{2S+1}l_n k_3 l_3 \ ^2\mathcal{L} \rightarrow k_1 l_1 k_2 l_2 \ ^{2S+1}l_n k_3 l_3 \ ^2\mathcal{L}$  is given by

$$V_{fi} = \delta_{l_0, \mathcal{L}} \sum_{k_n} (-1)^{l_1-l_2} \begin{pmatrix} l_1 & l_2 & l_n \\ 0 & 0 & 0 \end{pmatrix} (-1)^{l_n-l_3} \begin{pmatrix} l_n & l_3 & l_0 \\ 0 & 0 & 0 \end{pmatrix} \times \left( \sqrt{\frac{(2l_2+1)}{(2l_1+1)}} R^{l_1}(k_1 l_1, k_2 l_2, 1s, k_n l_n) + (-1)^s \sqrt{\frac{(2l_1+1)}{(2l_2+1)}} R^{l_2}(k_1 l_1, k_2 l_2, k_n l_n, 1s) \right) \times \left( \sqrt{2} \delta_{s,0} \sqrt{\frac{(2l_3+1)}{(2l_n+1)}} R^{l_n}(k_n l_n, k_3 l_3, 1s, k_0 l_0) \right)$$

TABLE V. Electron-impact single ionization cross sections (in kb), leaving He<sup>+</sup> in the 1s ground state, as calculated by the frozen-core 2D time-dependent close-coupling method [12], at various incident electron energies (1.0 kb = 10 × 10<sup>-21</sup> cm<sup>2</sup>).

$\mathcal{L}$	100.0 eV	150.0 eV	200.0 eV
0	1860	1270	920
1	3230	2340	1760
2	5550	3760	2720
3	6180	4630	3470
4	5560	4720	3740
5	4360	4250	3600

$$- \sqrt{\frac{(2S+1)}{2}} \sqrt{\frac{(2l_n+1)}{(2l_3+1)}} R^{l_3}(k_n l_n, k_3 l_3, k_0 l_0, 1s) \times \left( E_{atom} + \frac{k_0^2}{2} - E_{ion}(1s) - \frac{k_n^2}{2} - \frac{k_3^2}{2} \right)^{-1}. \quad (20)$$

The 1s and  $nl_n$  bound orbitals are hydrogenic, while the  $k_0 l_0$ ,  $k_1 l_1$ ,  $k_2 l_2$ ,  $k_3 l_3$ , and  $k_n l_n$  continuum orbitals are calculated in a  $V^{N-2}$  scattering potential. We note that in both Eqs. (17) and (20) the symbol  $\sum_{k_n}$  is shorthand for a sum over all  $n$  bound

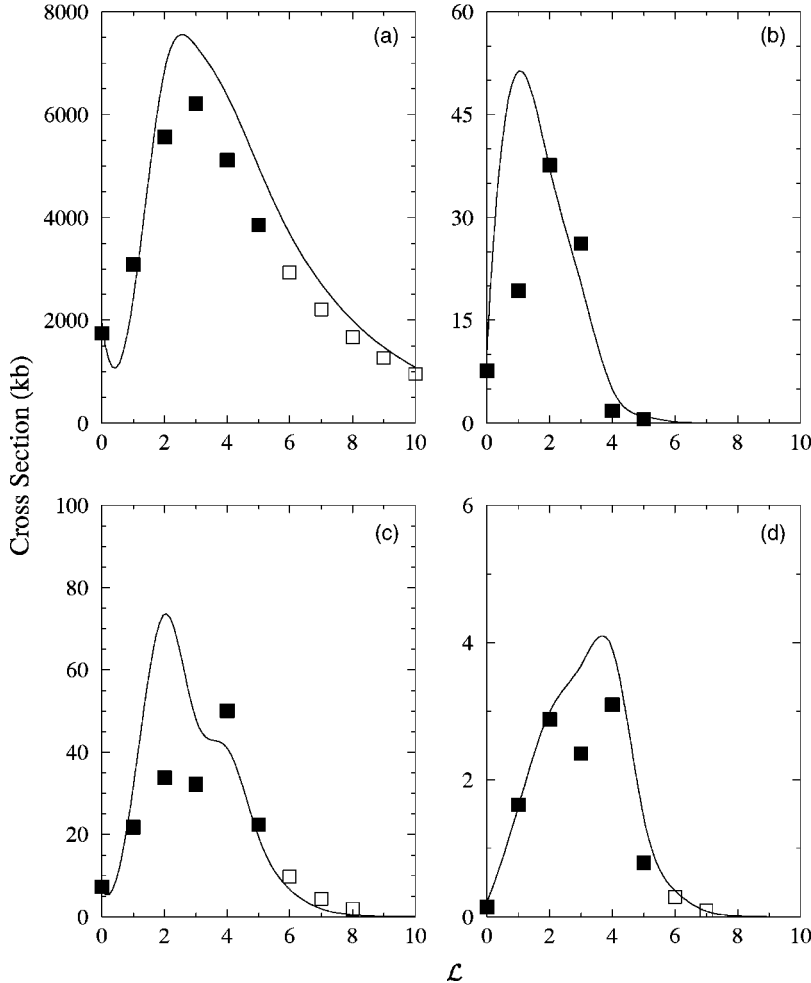


FIG. 1. Total cross sections per partial wave  $\mathcal{L}$  with an incident electron energy of 100 eV. (a) Single ionization, leaving He<sup>+</sup> in the 1s ground state, (b) single ionization, leaving He<sup>+</sup> in the 2s excited state, (c) single ionization, leaving He<sup>+</sup> in the 2p excited state, and (d) double ionization. Filled squares: time-dependent close-coupling calculations; open squares: extrapolated values; solid curves: time-independent distorted-wave calculations, scaled by factors of 1.00, 0.45, 0.37, and 0.11, respectively (1 kb = 10<sup>-21</sup> cm<sup>2</sup>).

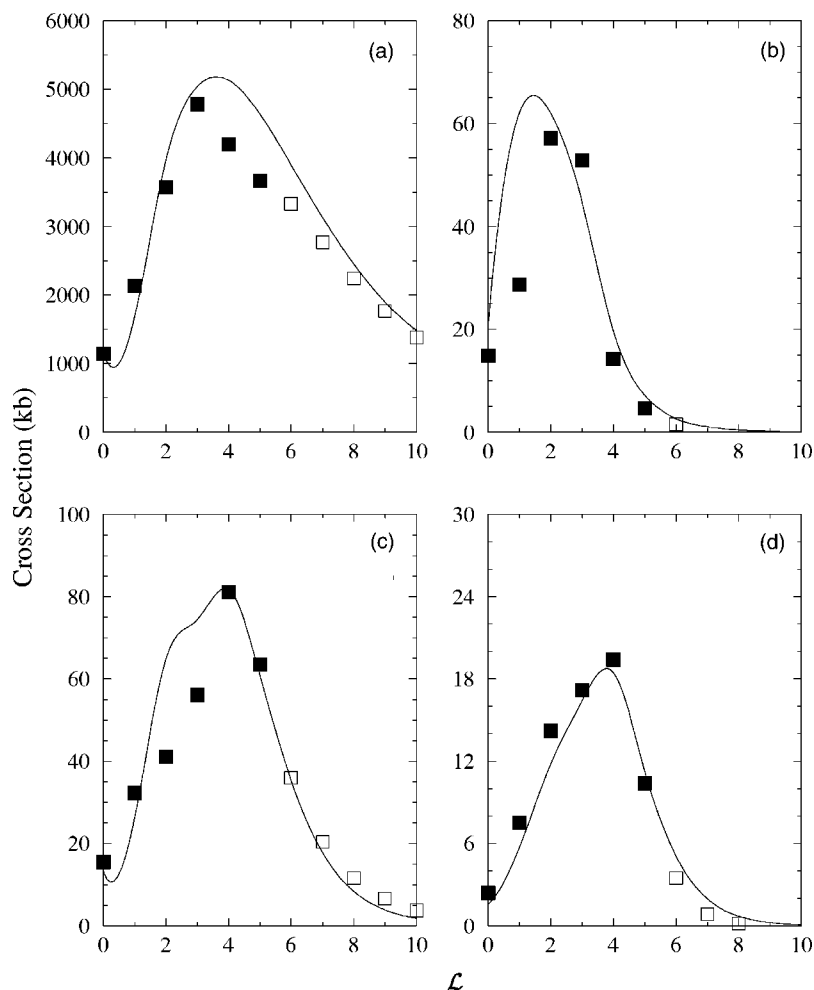


FIG. 2. Total cross sections per partial wave  $\mathcal{L}$  with an incident electron energy of 150 eV. (a) Single ionization, leaving  $\text{He}^+$  in the  $1s$  ground state, (b) single ionization, leaving  $\text{He}^+$  in the  $2s$  excited state, (c) single ionization, leaving  $\text{He}^+$  in the  $2p$  excited state, and (d) double ionization. Filled squares: time-dependent close-coupling calculations; open squares: extrapolated values; solid curves: time-independent distorted-wave calculations, scaled by factors of 1.00, 0.45, 0.37, and 0.11, respectively ( $1 \text{ kb} = 10^{-21} \text{ cm}^2$ ).

orbitals and an integral over all  $k_n$  continuum orbitals. The singularity in the denominator in both Eqs. (17) and (20) is handled by standard evaluation of a principal value integration and an imaginary term.

The important transition chosen for single ionization with excitation in Eq. (17) and double ionization in Eq. (20) represents the process of single ionization of helium followed by excitation or ionization of  $\text{He}^+$  by the outgoing ejected electron. Certainly, more second- and higher-order processes need to be considered in the scattering potential  $V_{fi}$  for a complete perturbative description. For our purposes, as will be seen in the following section, we plan to scale the perturbation theory cross sections to match the nonperturbative theory cross sections at low  $\mathcal{L}$ , and then extrapolate the nonperturbative results using the high  $\mathcal{L}$  scaled distorted-wave results as a guide.

### III. CROSS-SECTION RESULTS

The electron-impact single and double ionization cross sections for the  $1S$  ground state of helium were calculated at incident electron energies above the double ionization threshold. A  $(192)^3$  lattice was employed with each radial direction from  $0.0 \rightarrow 38.4$  spanned by a uniform mesh with

spacing  $\Delta r = 0.20$ . Initially the wave packet of Eq. (6) was centered at  $r_3 = 20.0$  with a coordinate space spread of 6.0. After relaxation to obtain a fully correlated ground state of helium on the lattice, the time-dependent close-coupled equations of Eq. (1) were propagated for up to 6200 time steps to obtain total cross sections from Eq. (11).

Single ionization cross sections are presented in Tables I–III, while double ionization cross sections are presented in Table IV. For  $\mathcal{L} = 0$ , 3 target channels [ $ss$ ,  $pp$ , and  $dd$ ] were used to obtain the two-electron wave function for the ground state of helium, 11 coupled channels [ $(ss)Ss$ ,  $(sp)Pp$ ,  $(ps)Pp$ ,  $(pp)Ss$ ,  $(sd)Dd$ ,  $(ds)Dd$ ,  $(dd)Ss$ ,  $(pp)Dd$ ,  $(pd)Pp$ ,  $(dp)Pp$ , and  $(dd)Dd$ ] were used to propagate the three-electron wave function by Eq. (1), and 10 determinantal projection functions [ $(ss)^1Ss$ ,  $(ss)^3Ss$ ,  $(sp)^1Pp$ ,  $(sp)^3Pp$ ,  $(sd)^1Dd$ ,  $(sd)^3Dd$ ,  $(pp)^1Dd$ ,  $(pp)^3Dd$ ,  $(dd)^1Dd$ , and  $(dd)^3Dd$ ] were used to determine the cross sections by Eq. (11). For example, the determinantal projection functions  $(sp)^{1,3}Pp$  will have nonzero overlap with the  $(sp)Pp$ ,  $(ps)Pp$ , and  $(pp)Ss$  coupled channels. Increasing the target channels by one to [ $ss$ ,  $pp$ ,  $dd$ , and  $ff$ ], the coupled channels to 23, and the determinantal projection functions to 16 had, at most, a 2% effect on the  $\mathcal{L} = 0$  single and double ionization cross sections at the three incident energies. Tables I–IV were completed using 3 target channels and 21 coupled channels for  $\mathcal{L} = 1$ , 23 coupled channels for  $\mathcal{L} = 2$ , 49 coupled channels for  $\mathcal{L} = 3$ , 63 coupled

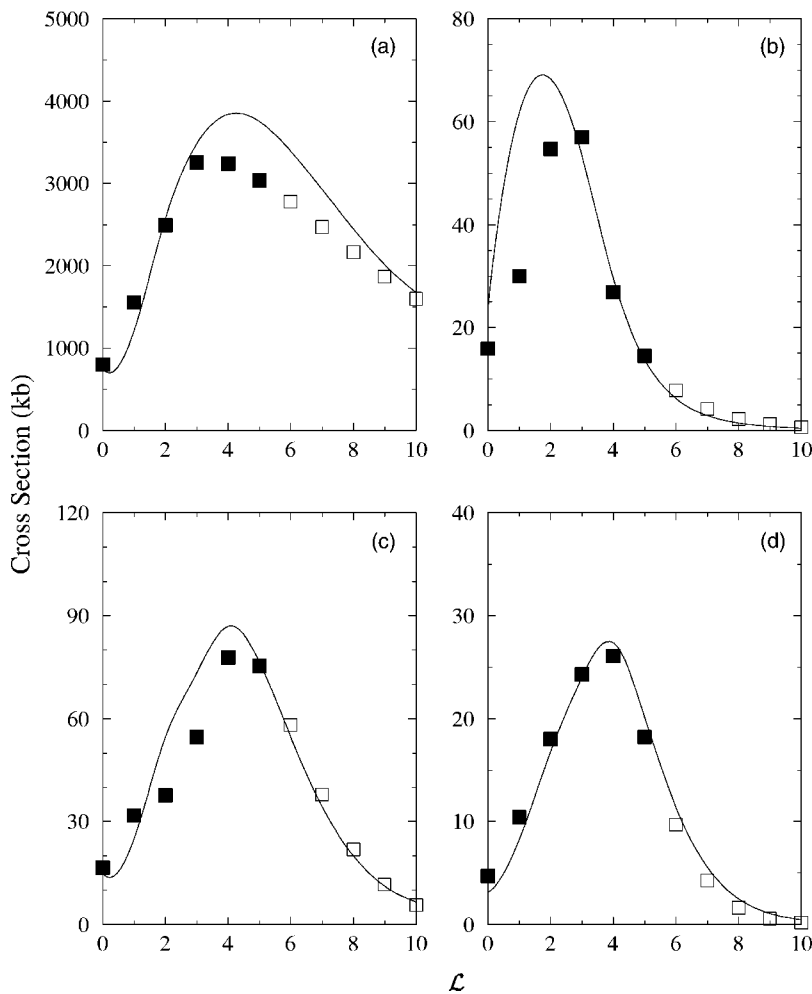


FIG. 3. Total cross sections per partial wave  $\mathcal{L}$  with an incident electron energy of 200 eV. (a) single ionization, leaving  $\text{He}^+$  in the  $1s$  ground state, (b) single ionization, leaving  $\text{He}^+$  in the  $2s$  excited state, (c) single ionization, leaving  $\text{He}^+$  in the  $2p$  excited state, and (d) double ionization. Filled squares: time-dependent close-coupling calculations; open squares: extrapolated values; solid curves: time-independent distorted-wave calculations, scaled by factors of 1.00, 0.45, 0.37, and 0.11, respectively ( $1 \text{ kb} = 10^{-21} \text{ cm}^2$ ).

channels for  $\mathcal{L}=4$ , and 87 coupled channels for  $\mathcal{L}=5$ . After increasing the target channels to 4, additional calculations were made at 200-eV incident energy involving 51 coupled channels for  $\mathcal{L}=1$ , 65 coupled channels for  $\mathcal{L}=2$ , and 65 coupled channels for  $\mathcal{L}=3$ . Again, only a small change in the  $\mathcal{L}=1,2,3$  single and double ionization cross sections was found. Currently, we find ourselves resource limited on checking channel coupling convergence for  $\mathcal{L}=4$  and  $\mathcal{L}=5$ . However, as a further check on the single ionization cross sections, leaving  $\text{He}^+$  in the  $1s$  ground state, previous frozen-core two-dimensional (2D) time-dependent close-coupling results [12] are presented in Table V. Comparing the 3D results from Table I with the frozen-core 2D results from Table V, we find that the 3D results are usually lower than the frozen-core 2D results. For example, at 200-eV incident energy, the 3D results are lower than the frozen-core 2D results by 13% for  $\mathcal{L}=0$ , 11% for  $\mathcal{L}=1$ , 8% for  $\mathcal{L}=2$ , 6% for  $\mathcal{L}=3$ , 13% for  $\mathcal{L}=4$ , and 16% for  $\mathcal{L}=5$ . At low  $\mathcal{L}$  the differences are probably due to the superiority of the full two-electron target wave function for helium found in the 3D results, while the increasing differences at high  $\mathcal{L}$  are probably due to the need for more coupled channels. With some uncertainty in the overall accuracy of the  $\mathcal{L}=4$  and  $\mathcal{L}=5$  results, we have limited our ionization calculations to the relatively low incident energies presented in the Tables (i.e., less than or equal to 200 eV). Thus, since for low energies

the higher partial waves contribute less, the total ionization cross-section accuracy should still be quite good.

To obtain total cross sections, we must extrapolate our time-dependent close-coupling results to large angular momentum  $\mathcal{L}$ . We show in Figs. 1–3 the total cross sections per partial wave for single and double ionization at 100-, 150-, and 200-eV incident energies, respectively. The filled squares are the present time-dependent close-coupling results from Tables I–IV and the open squares are obtained by our extrapolation method. In Figs. 1–3 the solid curves are time-independent distorted-wave calculations. For single ionization, leaving  $\text{He}^+$  in the  $1s$  ground state, the distorted-wave results are obtained from Eqs. (12)–(14) with unit scaling and are identical to previous results [12]. For single ionization, leaving  $\text{He}^+$  in the  $2s$  excited state, the distorted-wave results are obtained from Eqs. (15)–(17) scaled by a factor of 0.45. For single ionization, leaving  $\text{He}^+$  in the  $2p$  excited state, the distorted-wave results are obtained from Eqs. (15)–(17) scaled by a factor of 0.37. For double ionization, the distorted-wave results are obtained from Eqs. (18)–(20) scaled by a factor of 0.11. The distorted-wave scaling factors are simply chosen to help guide extrapolation of the much more accurate time-dependent close-coupling results to high angular momentum. In extrapolating our time-dependent results to larger  $\mathcal{L}$ , we choose a fitting function of the form

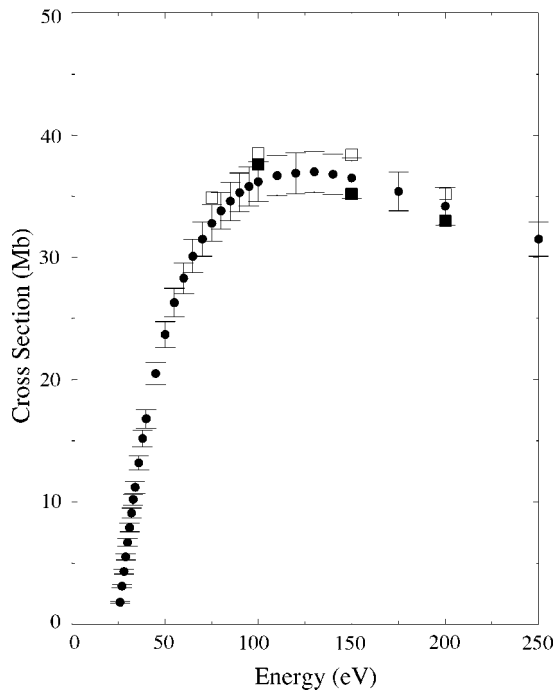


FIG. 4. Single ionization of helium, leaving  $\text{He}^+$  in the  $1s$  ground state. Filled squares: 3D time-dependent close-coupling calculations; open squares: frozen-core 2D time-dependent close-coupling calculations [12]; filled circles with error bars: absolute experimental measurements [13] ( $1 \text{ Mb} = 10^{-18} \text{ cm}^2$ ).

$$f(\mathcal{L}) = A(\mathcal{L} - \mathcal{L}_0)^n e^{-b\mathcal{L}}, \quad (21)$$

where  $A$ ,  $\mathcal{L}_0$ ,  $n$ , and  $b$  are varied to provide the best agreement, according to least squares criterion, between the time-dependent close-coupling results defining the peak of the cross section and the scaled distorted-wave results at higher  $\mathcal{L}$ . We employ this extrapolation method to obtain total ionization cross sections for all processes at incident energies of 100, 150, and 200 eV.

Total single ionization cross sections, leaving  $\text{He}^+$  in the  $1s$  ground state, are shown in Fig. 4. The present 3D time-dependent calculations are represented as filled squares, frozen-core 2D time-dependent calculations [12] are shown as open squares, and absolute experimental measurements [13] are filled circles with error bars. The 3D results are slightly lower than the frozen-core 2D results, but both calculations are within the error bars of the absolute experimental measurements. Total single ionization cross sections, leaving  $\text{He}^+$  in the  $2s$  excited state, are shown in Fig. 5. The time-dependent close-coupling results are shown as filled squares, while the hybrid distorted-wave/ $R$ -matrix calculations [17] are shown as the solid curve. The time-dependent results are found to rise faster as a function of incident energy than the hybrid results, reaching a maximum difference of about 50% at 200 eV. Total single ionization cross sections, leaving  $\text{He}^+$  in the  $2p$  excited state, are shown in Fig. 6. The time-dependent close-coupling results are shown as filled squares, and lie between the absolute experimental measurements [18,19] and the hybrid distorted-wave/ $R$ -matrix calculations [17]. Finally, total double ionization

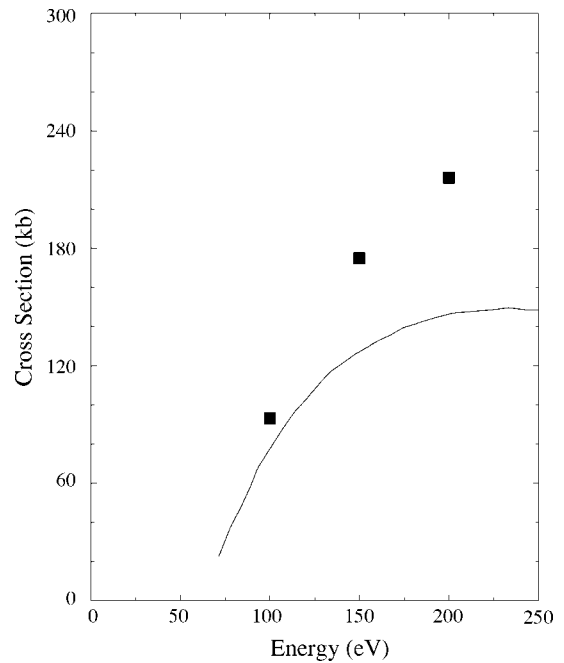


FIG. 5. Single ionization of helium, leaving  $\text{He}^+$  in the  $2s$  excited state. Filled squares: 3D time-dependent close-coupling calculations; solid curve: hybrid distorted-wave/ $R$ -matrix calculations [17] ( $1 \text{ kb} = 10^{-21} \text{ cm}^2$ ).

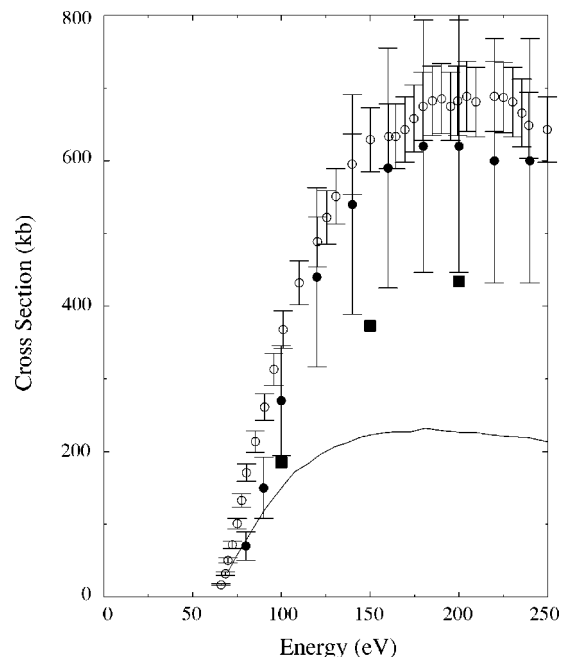


FIG. 6. Single ionization of helium, leaving  $\text{He}^+$  in the  $2p$  excited state. Filled squares: 3D time-dependent close-coupling calculations; solid curve: hybrid distorted-wave/ $R$ -matrix calculations [17]; filled circles with error bars: absolute experimental measurements [18]; and open circles with error bars: absolute experimental measurements [19] ( $1 \text{ kb} = 10^{-21} \text{ cm}^2$ ).

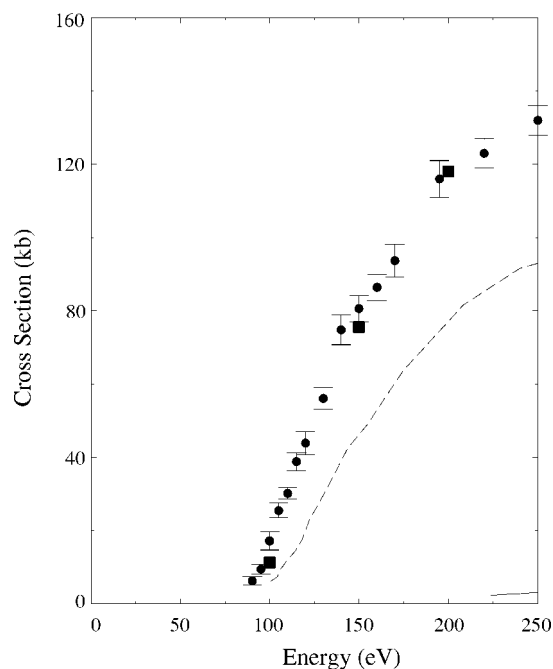


FIG. 7. Double ionization of helium. Filled squares: 3D time-dependent close-coupling calculations; dashed curve: hybrid plane-wave/distorted-wave calculations with no final state correlations [20]; solid curve: hybrid plane-wave/distorted-wave calculations with final-state correlations [20]; filled circles with error bars: absolute experimental measurements [15] ( $1 \text{ kb} = 10^{-21} \text{ cm}^2$ ).

cross sections are shown in Fig. 7. The time-dependent close-coupling results are shown as filled squares, hybrid plane-wave/distorted-wave calculations [20] are shown as the dashed and solid curves, and absolute experimental measurements [15] are filled circles with error bars. The time-dependent close-coupling results are found to lie within the error bars of the absolute experimental measurements. We note that the hybrid results shown in Fig. 7 that do not in-

clude final state correlation effects (dashed curve) are much higher than those calculations (solid curve) that do include final-state correlation effects [20].

#### IV. SUMMARY

In conclusion, we find that a nonperturbative lattice solution of the time-dependent Schrödinger equation appears capable of yielding accurate cross sections for Coulomb four-body breakup. The double ionization cross sections for helium are found to be in excellent agreement with absolute experimental measurements, extending up to incident electron energies of 2.5 times threshold. For higher energies, some uncertainty in the overall accuracy of the present  $\mathcal{L}=4$  and  $\mathcal{L}=5$  partial wave cross sections becomes a limiting factor. Much work remains to be done in extending the present time-dependent close-coupling calculations to those higher energies at which the hybrid distorted-wave/ $R$ -matrix methods should become reasonably accurate. Convergence studies as a function of the number of coupled channels and the number of determinantal projection states need to be made for the higher partial waves, in which the lattice size is also varied. In addition, methods developed to calculate energy and angle differential cross sections for three-body Coulomb breakup [8] need to be generalized to four-body Coulomb breakup. The new and rich world of  $(e, 3e)$  four-body Coulomb phenomena awaits exploration by a full nonperturbative quantum theory.

#### ACKNOWLEDGMENTS

This work was supported in part by a grant for Scientific Discovery through Advanced Computing (SciDAC) from the U.S. Department of Energy. Computational work was carried out at the National Energy Research Scientific Computing Center in Oakland, California, and at the Center for Computational Sciences in Oak Ridge, Tennessee.

- 
- [1] I. Bray and A. T. Stelbovics, *Phys. Rev. Lett.* **70**, 746 (1993).  
 [2] D. Kato and S. Watanabe, *Phys. Rev. Lett.* **74**, 2443 (1995).  
 [3] K. Bartschat and I. Bray, *J. Phys. B* **29**, L577 (1996).  
 [4] M. S. Pindzola and F. J. Robicheaux, *Phys. Rev. A* **54**, 2142 (1996).  
 [5] M. Baertschy, T. N. Rescigno, W. A. Isaacs, X. Li, and C. W. McCurdy, *Phys. Rev. A* **63**, 022712 (2001).  
 [6] M. B. Shah, D. S. Elliot, and H. B. Gilbody, *J. Phys. B* **20**, 3501 (1987).  
 [7] T. N. Rescigno, M. Baertschy, W. A. Isaacs, and C. W. McCurdy, *Science* **286**, 2474 (1999).  
 [8] J. P. Colgan, M. S. Pindzola, F. J. Robicheaux, D. C. Griffin, and M. Baertschy, *Phys. Rev. A* **65**, 042721 (2002).  
 [9] I. Bray, *Phys. Rev. Lett.* **89**, 273201 (2002).  
 [10] D. V. Fursa and I. Bray, *Phys. Rev. A* **52**, 1279 (1995).  
 [11] E. T. Hudson, K. Bartschat, M. P. Scott, P. G. Burke, and V. M. Burke, *J. Phys. B* **29**, 5513 (1996).  
 [12] M. S. Pindzola and F. J. Robicheaux, *Phys. Rev. A* **61**, 052707 (2000).  
 [13] R. K. Montague, M. F. A. Harrison, and A. C. H. Smith, *J. Phys. B* **17**, 3295 (1984).  
 [14] R. C. Wetzel, F. A. Baiocchi, T. R. Hayes, and R. S. Freund, *Phys. Rev. A* **35**, 559 (1987).  
 [15] M. B. Shah, D. S. Elliott, P. McCallion, and H. B. Gilbody, *J. Phys. B* **21**, 2751 (1988).  
 [16] K. Bartschat and P. G. Burke, *J. Phys. B* **20**, 3191 (1987).  
 [17] A. Raeker, K. Bartschat, and R. H. G. Reid, *J. Phys. B* **27**, 3129 (1994).  
 [18] J. L. Forand, K. Becker, and J. W. McConcey, *J. Phys. B* **18**, 1409 (1985).  
 [19] P. A. Hayes and J. F. Williams, *Phys. Rev. Lett.* **77**, 3098 (1996).  
 [20] P. Defrance, T. M. Kereselidze, Z. S. Machavariani, and I. L. Noselidze, *J. Phys. B* **33**, 4323 (2000).  
 [21] A. Kheifets, I. Bray, A. Lahmam-Bennani, A. Duquet, and I. Taouil, *J. Phys. B* **32**, 5047 (1999).

- [22] P. J. Marchalant, J. Rasch, C. T. Whelan, D. H. Madison, and H. R. J. Walters, *J. Phys. B* **32**, L705 (1999).
- [23] Y. Fang and K. Bartschat, *J. Phys. B* **34**, L19 (2001).
- [24] M. S. Pindzola and F. J. Robicheaux, *Phys. Rev. A* **57**, 318 (1998).
- [25] M. S. Pindzola, F. J. Robicheaux, N. R. Badnell, and T. W. Gorczyca, *Phys. Rev. A* **56**, 1994 (1997).
- [26] D. M. Mitnik, M. S. Pindzola, D. C. Griffin, and N. R. Badnell, *J. Phys. B* **32**, L479 (1999).
- [27] J. P. Colgan, M. S. Pindzola, D. M. Mitnik, D. C. Griffin, and I. Bray, *Phys. Rev. Lett.* **87**, 213201 (2001).
- [28] C. W. McCurdy, D. A. Horner, and T. N. Rescigno, *Phys. Rev. A* **65**, 042714 (2002).
- [29] C. F. Fischer, *Comput. Phys. Commun.* **43**, 355 (1987).
- [30] S. M. Younger, *Phys. Rev. A* **22**, 111 (1980).